Materials and Design 47 (2013) 1–8

Contents lists available at SciVerse ScienceDirect

Materials and Design

journal homepage: www.elsevier.com/locate/matdes

Austenitic and ferritic stainless steel dissimilar weld metal evaluation for the applications as-coating in the petroleum processing equipment

Cleiton C. Silva [a,*], Hélio C. Miranda [a], Hosiberto B. de Sant'Ana [b], Jesualdo P. Farias [a]

[a] Universidade Federal do Ceará, Department of Materials and Metallurgical Engineering, Campus do Pici, Building 715, Fortaleza, Ceará, Brazil
[b] Universidade Federal do Ceará, Department of Chemical Engineering, Campus do Pici, Building 709, Fortaleza, Ceará, Brazil

ARTICLE INFO

Article history:
Received 5 August 2012
Accepted 24 November 2012
Available online 5 December 2012

Keywords:
Stainless steel
High temperature corrosion
Acid corrosion
Welding

ABSTRACT

The current study presents some fundamental observations on the effects of the welding heat input in the chemical composition, microstructure, hardness and petroleum corrosion resistance of the fusion zone, formed by the AWS E309MoL austenitic stainless steel covered electrode and the AISI 410S ferritic stainless steel, being a dissimilar welding procedure. Such welding configurations are widely used as an overlay of equipment in the petroleum and gas industries. The welds were performed with the application of three different levels in heat inputs (6, 9 and 12 kJ/cm). Samples of the weld metals were conventionally prepared for the microstructural characterization by light microscopy and scanning electron microscopy. A corrosion test with samples immersed in heavy oil heated at 300 °C, was carried out for a period of 60 h. The corrosion rate was determined by the weight loss given after the aforesaid test. The fusion zone microstructure has a typical δ-ferrite acicular morphology, from which the level of δ-ferrite was duly altered with the increases of the welding heat input, due to the variations in the composition of the weld metal caused by dilution. It was also concluded that the chemical composition and the weld metal microstructure had a slight influence in the material's corrosion rate. As a matter of fact, the corrosion rate of the weld metals evaluated herein, was considered satisfactory with few variations between the welding heat inputs duly applied.

1. Introduction

The welding process is widely used in the constructions and repairs of equipments in the gas and petroleum industries. In the petroleum distillation towers, these said weldings can be used, in order to apply lining coatings or weld overlays in internal surfaces [1]. In this type of repair, the base metal is usually the original stainless steel clad, which covers internal surface of the equipment.

One particular example of the material which has been used as a clad of the petroleum distillation towers, are the ferritic stainless steels, due to its good resistance to localized corrosion (pits and crevice) and excellent stress corrosion cracking [2]. Among several ferritic stainless steels it can be pointed the AISI 410S which has a chemical composition basically composed by 11–12% of chromium. This stainless steel is derived from AISI 410 martensitic stainless steel, however, its microstructure is completely ferritic, instead of martensitic due to a lower carbon content and a controlled cooling rate. In the decade of the 1970s, some equipments were constructed using AISI 410S ferritic stainless steel as cladding, mainly due to the low corrosivity of the crude oil processed in this period. The advantages of the use of this stainless steel were based on its lower cost if compared with other classes of stainless steels and due to its physical properties, specially thermal expansion coefficient and thermal conductibility, which are near the structural ferritic steels. These characteristics avoid the occurrence of some problems associated to thermal fatigue.

As commented before, the above steel was considered in projects of distillation towers for the older petroleum refineries, destined to the processing of high quality oil with a low acid level. Nevertheless, with the discovery of new petroleum fields with heavy oil and extreme acid, however economically attractive, this particular oil started to be processed in the refinering settings. As result, an intense corrosive process was observed in some equipments, especially in distillation towers, which are innerly coated by the AISI 410S ferritic stainless steels.

To restore these equipments and to guarantee a good performance in operations, the inner surface corroded are again coated with the application of linings derived from the ferritic and/or austenitic stainless steel, especially those containing high chromium levels and addition of molybdenum, as types 444, 316L and 317L [3–5]. Another possibility to recover the degraded surfaces is the weld overlay, in which one or more layers are deposited on the surface using a corrosion resistant alloy consumable.

In this context, three distinct zones are formed during welding: fusion zone (FZ), partial melted zone (PMZ) and a heat affected

* Corresponding author. Tel.: +55 85 33669358; fax: +55 85 33669969.
E-mail address: cleiton@metalmat.ufc.br (C.C. Silva).

0261-3069/$ - see front matter © 2012 Elsevier Ltd. All rights reserved.
http://dx.doi.org/10.1016/j.matdes.2012.11.048

zone (HAZ) [6,7]. In many of the cases, the heat affected zone is the most critical due to the metallurgical changes caused by the welding heat cycle [8–11]. However, other parts of the welded joint may have significant metallurgical changes, such as the fusion zone, being needed a careful evaluation of its characteristics.

As a general rule, the ferritic stainless steels are subjected to excessive grain growth in the fusion zone and heat affected zone [12,13]. This behavior is mainly due to the complete solidification in ferrite mode and negligible phase transformation in the solid state which could help the grain refinement [14]. In fact, after the weld solidification of the 11% Cr ferritic stainless steels a net of austenite is formed along the ferrite grain boundaries at high temperatures, which transformers in martensite on cooling [7]. Nonetheless, this phase transformation is insufficient to avoid the grain growth. Because of the grain coarsening and formation of martensite along the ferrite grain boundaries these ferritic stainless steel welds exhibit poor toughness, ductility and corrosion resistance [14,15].

In order to apply these linings or weld overlays and to overcome these undesirable situations, the welding procedure for ferritic stainless steels recommends the use of austenitic filler metals, resulting in a dissimilar ferritic/austenitic stainless steel weld metal [16–19]. In the petroleum, gas and petrochemical industries the AWS E309MoL-16 covered electrodes are frequently utilized for both linings and overlay applications due to high content of alloying elements such chromium, nickel and addition of molybdenum above 2 wt.% [3,20]. The resultant chemical composition of the fusion zone is related to the degree of mixing between filler metal and base metal (dilution level).

In this case, a biphasic microstructures constituted by austenite plus δ-ferrite is expected. However, the proportion in δ-ferrite and morphology may varying significantly depending on the percentage of ferritizing and austenitizing elements, as well as the cooling rate [21,22]. Despite progress in the study of the effects in the stainless steel weld metal's microstructure and its mechanical properties, little is known regarding the influence of the solidification mode and the δ-ferrite content, as well as the morphology on the corrosion resistance weld metals, encouraging the development of studies in this area, especially when the microstructural changes are so expressive, due to the aspects of dilution and high cooling rates.

Therefore, knowledge of the corrosion resistance in the materials applied as linings and weld overlays in the equipments that process heavy oil, especially distillation towers, should not be restricted to the study of the HAZ [4,10,23], since the fusion zone can also represent a critical zone. This particular study evaluated the microstructure and corrosion behavior caused by the Brazilian heavy oil in the dissimilar weld metals, between the AWS E309MoL-16 austenitic stainless steel covered electrode diluted with AISI 410S ferritic stainless steel.

2. Materials and methods

2.1. Crude oil characterization

The crude oil used in this study (a heavy oil from Campos Basin in Rio de Janeiro, without any pre-processing), was supplied by the Leopoldo Américo M. de Mello Center for Research and Development – CENPES/Petrobras. The physical properties of the petroleum used are presented in Table 1.

2.2. Base metal and filler metal characterization

The base metal used in this study was a cold rolled plate of AISI 410S ferritic stainless steel with 3 mm thickness. The chemical composition determined by optical emission spectroscopy is presented in Table 2. To confirm the ferritic microstructure a test specimen was extracted from the plate and prepared to metallographic evaluation, being observed using optical microscopy, as shown in Fig. 1. The filler metal used was the AWS E 309MoL-16 austenitic stainless steel covered electrode with a diameter of 2.5 mm. The chemical composition of the filler metal was determined by optical emission spectroscopy and is presented in Table 3.

2.3. Welding procedure

Weldings were performed by the shielding metal arc welding (SMAW) process in flat position on the AISI 410S ferritic stainless steel plates, measuring 50 × 150 mm and 3.0 mm thick. The procedure was carried out manually and the welding speed was controlled using an Automatic Positioner for Experimental Welds with the Covered Electrode, developed by the "*Laboratório de Engenharia de Soldagem*" (Engineering Welding Laboratory) at the Federal University of Ceará. A multi-process welding supply, being the INVERSAL 450 was used together with a data acquisition system (arc current and voltage). Three levels of welding heat input were used in this study; their parameters are shown in Table 4.

2.4. Thermal treatments

After welding the process, the plates were cleaned in order to remove the slag. Next to the plates, there were cuts to extract 12 × 25 × 3.0 mm in samples from the welded metal. The samples were submitted to a thermal treatment immersed in crude oil, at 300 °C. This treatment in heavy oil lasted 60 h. It is noteworthy that these test conditions are apparently less severe than those in distillation towers, in which apart from the effects of temperature and oil corrosiveness, there are the action of stresses and fluid flows, among other factors in the effect of the corrosion process of in the material used with the coating.

2.5. Metallurgical analysis

After the welding, samples were extracted from the plates and conventionally prepared for metallographic analysis in the sections transverse to the welding direction. These samples were analyzed using the optical microscopy (OM), scanning electron microscope (SEM) and energy dispersive X-ray spectroscopy (EDS). This said samples were etching with Vilela's reagent (1 g of picric acid, 100 mL of ethylic alcohol and 5 mL of chloridric acid).

The delta ferrite quantify was carried out through two techniques: image analysis from the metallographic images and the ferritoscope (magnetic method). To evaluate the delta ferrite content by image analysis technique, 50 images for each weld metal were obtained by scanning electron microscopy. These images were processed and analyzed using a new solution software based on a multilayer neuronal network, which has been successful used

Table 1
Physico-chemistry analysis of the crude oil.

Gravity (20/40)	API	Viscosity at 50 °C (mm^2/s)	Sulfur (%m/m)
0.91042	16.8	240	0.56

Table 2
Chemistry composition of the AISI 410S stainless steel (wt.%).

C	Mn	Si	P	S	Cr	Ni
0.014	0.45	0.39	0.025	0.002	11.5	0.17

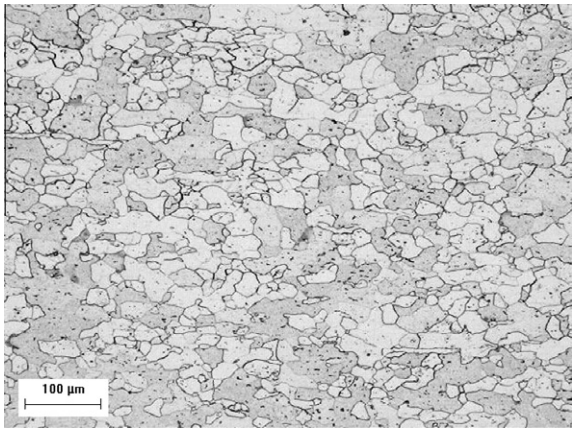

Fig. 1. Microstructure of AISI 410S base metal displaying a matrix completely ferritic and some particles of TiN.

Table 3
Chemistry composition of the electrode AWS E309MoL-16 (wt.%).

C	Mn	Si	P	S	Cr	Ni	Mo
0.04	1.10	0.90	0.03	0.01	23.9	12.1	2.4

Table 4
Welding parameters in CC⁺.

Current (A)	Voltage (V)	Welding speed (cm/min)	Welding heat input (kJ/cm)
80	25	20.0	6.0
80	25	12.5	9.0
80	26	10.0	12.0

for microstructural evaluation [24]. An example of micrograph obtained by SEM in secondary electron (SE) mode and used in image analysis is presented in Fig. 2a, as well as its respective segmented image (Fig. 2b). The delta ferrite content was also evaluated by a magnetic induction method, using a Ferritoscope® instrument, which was previously calibrated. The chemical composition of the weld metal was determined by optical emission spectroscopy.

2.6. Superficial characterization after thermal treatment

After treatment the samples were cleaned with kerosene for a subsequent evaluation of their surface. SEM and EDS analysis were used to identify the corrosion products present on the surface and the corrosion types, caused by heavy oil. The aforesaid samples were kept in a closed container, immersed in kerosene, until they were examined with the SEM. This condition was taken to avoid prolonged contact with the air, which could cause an atmospheric corrosion process.

2.7. Corrosion rate evaluation

In order to determine the velocity of the corrosion process and the aggressiveness of the corrosive environment, mass loss was determined through measurements of the sample's mass, before and after the heat treatment in heavy oil. The samples were submitted to clean chemical, using an alcohol solution with 20% of nitric acid during 10 min. A sample of each material as-welded (without petroleum treatment), was placed in acid together with the duly treated samples, in order to check whether there is a loss of mass due to the cleaning. However, none of the welded samples showed a loss in mass. The corrosion rate was determined by Eq. (1), following ASTM: G1-03.

$$\textit{Corrosion rate}\ (\text{mm/year}) = \frac{8.76 \times 10^4 \times W}{A \times D \times T} \quad (1)$$

where W is the weight loss in g; A is the surface area of the specimen in cm^2; D is the density of the material in g/cm^3; and T is the corrosion time in h.

3. Results and discussions

3.1. Microstructural characterization

3.1.1. Dilution evaluation

The weld metal dilution with the AISI 410S stainless steel base metal grew with the increase in the welding heat input, as shown in Fig. 3. The dilution level determined by the image analysis was initially used to estimate the chemical composition in the fusion zone. However, the possibility of more accuracy in the determination of the alloying elements contents in the welded metal, a chemical composition analysis by optical emission spectroscopy was carried out. The results are presented in Table 5. Based on the equations in WRC-1992 diagram, presented by Kotecki and Siewert [25] and Kotecki [26], Cr_{eq} – (Eq. (2)) – and Ni_{eq} (Eq. (3)), as well as the Cr_{eq}/Ni_{eq} ratio, were calculated and which are shown in Table 5.

$$Cr_{eq} = Ni + 35C + 20N + 0.25Cu \quad (2)$$

$$Ni_{eq} = Cr + Mo + 0.7Nb \quad (3)$$

Cr_{eq} reduces between 21.59% and 21.86%, and when compared with the Cr_{eq} for the pure weld metal (24.7%). This reduction in the values of Cr_{eq} is attributed to the low chromium content in the base metal (11.5 wt.% Cr) and the absence of the molybdenum. However, the main effect of dilution in the weld metal chemical composition is on Ni_{eq}, due to the AISI 410S ferritic stainless steel having a very low austenitizing element levels, such as nickel and carbon. Regarding the weld metal without dilution (pure filler metal), the reduction in the value of Ni varied between 8.54 wt.% and 7.39 wt.% with the increase in the welding heat input, which corresponds to a drop of 30–39% in Ni content approximately, when compared to 12.1 wt.% Ni content in the pure filler metal.

As a result, the Ni_{eq} decreased from 11.5 for the 6 kJ/cm to 10.22 for the 12 kJ/cm heat input. It is important to highlight that in this evaluation was considered the presence 0.08 wt.% N in the bulk of weld metal, which would be a typical value for AWS E309MoL-16 weld metal [27]. In this calculation it was considered that the austenite contains virtually all of the original nitrogen content of the weld metal, which is in agreement with Ogawa and Koseki [28] study in which it was demonstrated that the ferrite contains virtually 0 wt.% N. Thus was established in this study that the ferrite contains 0 wt.% N and the austenite will contain approximately 0.10 wt.% N, due to the presence of approximately 20% of ferrite.

It is observed that the drop in Ni_{eq} is more significant when compared to the reduction in Cr_{eq}, since the base metal contains some quantities of Cr (11.5 wt.%), however, the Ni content is residual (0.17 wt.%). Calculating the Cr_{eq}/Ni_{eq} ratio, we observed a slight difference in the values and a small tendency to increase with the increase in the heat input.

According the literature four distinct solidification modes may occur – fully austenitic (A); primary austenite and secondary ferrite (AF); primary ferrite and secondary austenite (FA); fully ferritic (F). In addition, after solidification a solid state transformations from the primary phase to a secondary phase may occur [29,30], therefore, resulting in a duplex structure being formed by austen-

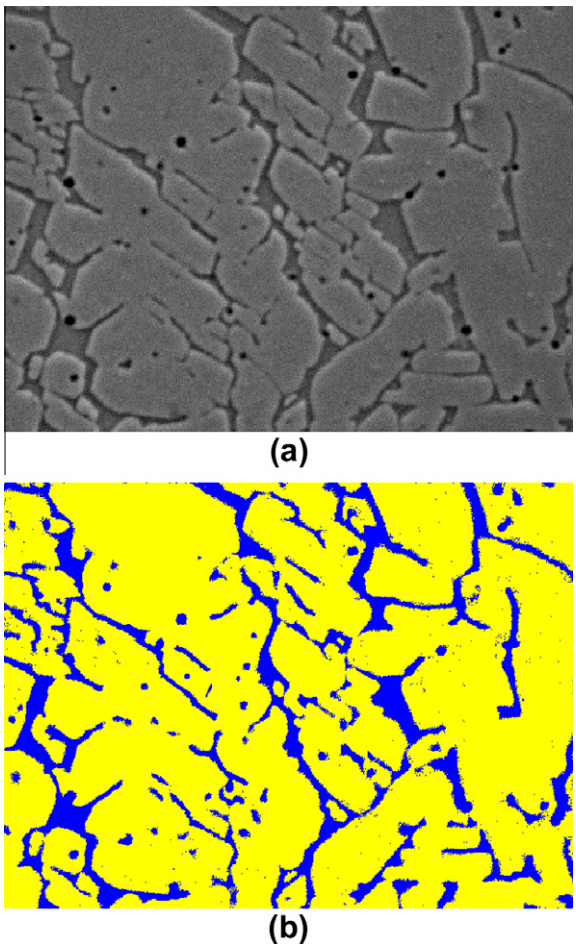

Fig. 2. (a) SEM micrograph using secondary electron mode used in image analysis. The data bar was intentionally removed. (b) Segmented image by the software based on a multilayer neuronal network.

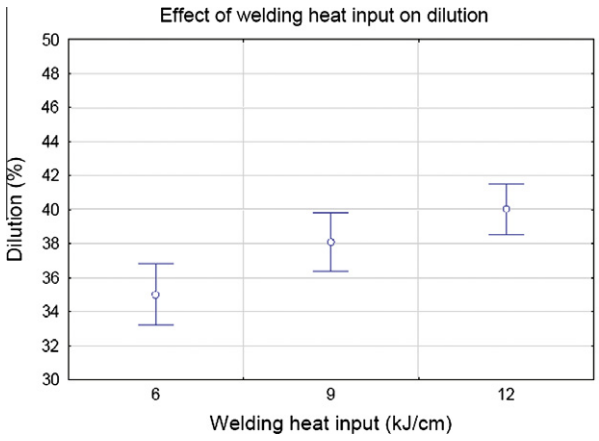

Fig. 3. Welding heat input effect on the dilution.

ite and ferrite. These solidification modes are shown in the pseudo-binary Fe–Cr–Ni diagram in Fig. 4.

Based on Cr_{eq}/Ni_{eq} ratio for the three weld heat inputs, which presented a slight difference, in all cases the results indicated that the weld metal was solidified in a completely ferritic mode, subsequently undergoing a solid state phase transformation from ferrite to austenite. This mode of solidification causes significant alterations in the δ-ferrite morphology, as can be seen in the next section.

The alterations in the values of Cr_{eq} and Ni_{eq} can have a higher influence on the δ-ferrite formation. Although there was a reduction in Cr_{eq}, and consequently a decrease in the percentage of the ferrite stabilizers elements, whereas the reduction in Ni_{eq} being more accentuated, which caused a significant reduction in the elements such as nickel and carbon, being strong promoters of austenite, leading to an increase in the δ-ferrite content.

3.1.2. Evaluation of the δ-ferrite content

The δ-ferrite content measured by image analysis and by a magnetic method, presents a tendency to grow with the increase of the welding heat input for both methods, as shown in Fig. 5. This increase in the δ-ferrite content is attributed to changes in the weld metal's chemical composition. Although the chemical composition undergoes a small reduction in the chromium level, the reduction in the nickel content for the joint is more significant and expressive in promoting δ-ferrite.

As in the ferrite–austenitic solidification mode, the completely ferritic solidification mode is also influenced by the cooling rate, which tends to increase the δ-ferrite content with increases in the cooling rate [22] and in the ferritic base metal (410S), due to its constitution and its chemical composition, which is rich in ferritizing elements and poor in austenite stabilizing elements. It is believed that the chemical composition is sufficient to offset the cooling rate effect, promoting a tendency for stabilizing the δ-ferrite in the weld metal and avoiding the ferrite-to-austenite solid state transformation with the increase of the welding heat input.

Based on the results of the chemical composition shown in Table 5 and using the WRC 1992 [25] diagram with the correspondent Cr_{eq} and Ni_{eq} equations, we also estimated the δ-ferrite, which are shown in Table 6. The results indicated that the δ-ferrite contents increase from 22 FN to 24 FN, when the heat input increase from 6 to 9 kJ/cm. Considering the increase in heat input from 9 to 12 kJ/cm, we observed again an increase in the δ-ferrite content, which was estimated in 29 FN. Comparing these results with measurement methods duly presented in this study, the values observed were considered very close, except to higher heat input conditions, in which the measurements showed a lower δ-ferrite content when compared to the WRC 1992 results. This behavior can be associated to the effect of the cooling rate, which is slower for higher heat input, proportioning more time to occur the δ-ferrite-to-austenite solid state transformation. Due to this probable effect which is not considered in constitution diagrams, the difference in measured and estimated results in the content of δ-ferrite was observed.

3.1.3. Morphology evaluation of the δ-ferrite

The δ-ferrite morphology in the pure weld metal was vermicular, being characteristic of austenitic stainless steel weld metals

Table 5
Dilution results and chemical composition of the weld metal (wt.%).

Welding heat input (kJ/cm)	C	Cr	Ni	Mo	Mn	Si	Nb	Cr_{eq}	Ni_{eq}	Cr_{eq}/Ni_{eq}
6	0.03	19.64	8.54	1.45	0.83	0.5	0.02	21.86	11.50	1.90
9	0.02	19.16	8.04	1.58	0.81	0.54	0.02	21.56	10.90	1.98
12	0.03	19.06	7.39	1.53	0.79	0.59	0.02	21.49	10.22	2.10

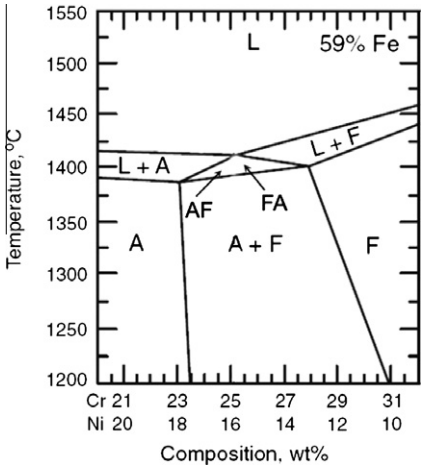

Fig. 4. Iron–chromium–nickel pseudo-binary diagram [22].

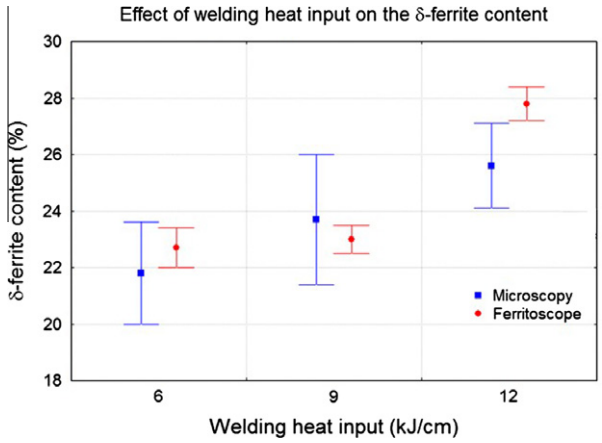

Fig. 5. Welding heat input effect on the δ-ferrite content.

solidifying in FA mode, as can be seen in Fig. 6a. However, due to the dilution between the filler metal and the base metal, the welds for the three heat input conditions tested in this study shows acicular δ-ferrite morphology, as shown in Fig. 6b–d. There is no consensus on the definition of this morphology among researchers. David [29] states that acicular morphology is characterized by a random arrangement of ferrite in the needle form, distributed on an austenitic matrix. Lippold and Savage [31], studied the effect of joints composition in the morphology of δ-ferrite. They defined this morphology as formed by acicular austenite in a ferritic matrix, circled almost completely by a net of austenite around the grain.

Although there are differences regarding the definition of acicular morphology, there is a consensus that this morphology is typical of the weld metal with a Cr_{eq}/Ni_{eq} ratio above 2. However, David [29] found the δ-ferrite with acicular morphology in welds whose Cr_{eq}/Ni_{eq} ratio was 1.66. The presence of this morphology was attributed to macrosegregations, causing localized variation in the chemical composition of the weld metal.

3.2. Corrosion evaluation in heavy petroleum

3.2.1. Superficial characterization

The superficial characterization in the weld metal obtained by SEM, is shown in Fig. 7. Fig. 7a and b, which shows the surface of the test samples welded using a heat input of 6 and 9 kJ/cm, showing some regions with a more attacked appearance, characterized by the formation of large amounts of corrosion products. Fig. 7c shows the surface of the weld metal where 12 kJ/cm of heat input was used. The whole surface of this particular sample, was covered by a layer of iron sulfide (Fig. 7d). Fig. 8a and b shows the details of the morphology of the layer from the corrosion product formed.

An important observation regarding the characterization of the corrosion products present on the surface of all the materials evaluated, was the chemical analysis obtained with EDS (Fig. 7d), showing the presence of high levels of sulfur and iron, indicating that the corrosion product present was iron sulfide. The formation of iron sulfide as a corrosion product, is a strong indication of corrosion processes associated to substances rich in sulfur, such as acids originating from sulfur compounds (especially hydrogen sulfide), as well as corrosion by naphthenic acids [32–34]. Another important factor influencing these corrosion processes in the equipments in the oil and gas industries, are the high temperatures in which these forms of corrosion occur, generally varying between 200 and 400 °C [35–38].

The petroleum used in this study has a high level of corrosiveness with a total acid number (TAN) above the minimum necessary for a potential corrosion problem by naphthenic acids. The temperature used in the test is high enough and within the range in which corrosion by hydrogen sulfide and by naphthenic acids is probable. The corrosion products are made up of iron sulfide, also a characteristic of corrosion by the both corrosion process. Thus, there are indicators that reinforces suspicions to the ones to be most probable, being the corrosion processes caused by heavy oil through naphthenic acids attacks. Additionally, the presence of sulfur (Table 1) is considered to encourage joint action between the naphthenic acids and hydrogen sulfide, therefore, resulting in an intense and complex corrosion process.

3.2.2. Corrosion evaluation

The corrosion rate practically did not vary; there was only a slight tendency to increase with the increase in the welding heat input (Fig. 9). These said welds, properly presented above, shows that dilution acts decisively in modifying the chemical composition, leading to significant microstructural alterations, such as variations in the level and morphology of δ-ferrite, when compared to the pure weld metal. However, it is possible that this variation does not influence the corrosion resistance as much.

The levels of chromium were reduced. The original presence of 24 wt.% of chromium dropped to 19.64 wt.%, 19.16 wt.% and 19.06 wt.%, respectively, due to the dilution for each welding heat input 6, 9 and 12 kJ/cm. As a matter of fact, the molybdenum levels vary expressively, remaining between 1.45% and 1.58%, below to the minimum levels recommended to promote a better satisfactory naphthenic acids corrosion resistance [37–39]. The element which varied with dilution was nickel, which drops from its original level

Table 6
Dilution results and δ-ferrite content in the weld metal.

Welding heat input (kJ/cm)	Dilution (%)		δ-Ferrite content		
	Image analysis	Chemical analysis	Microscopy (% δ-ferrite)	Ferritoscope (% δ-ferrite)	WRC 1992 (FN)
6	35	31	21.8 ± 1.8	22.7 ± 0.7	22
9	38	34	23.7 ± 2.3	23.0 ± 0.5	24
12	40	39	25.6 ± 1.5	27.8 ± 0.6	29

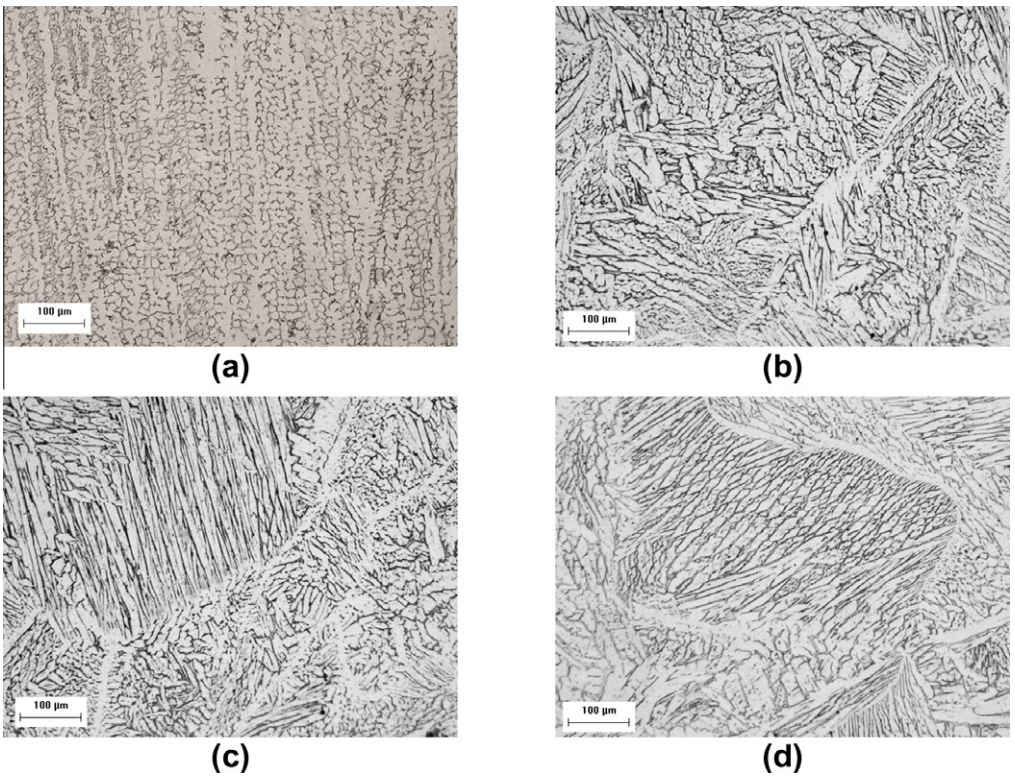

Fig. 6. (a) Microstructure of the pure AWS E309MoL filler metal showing austenite phase and δ-ferrite with vermicular morphology obtained by optical microscopy, etching: Vilelás reagent (200×). Microstructure of the weld metal AWS E 309MoL diluted with AISI 410S. (b) Welded with 6 kJ/cm. (c) Welded with 9 kJ/cm. (d) Welded with 12 kJ/cm. Etching: Vilela. Optical microscopy (200×).

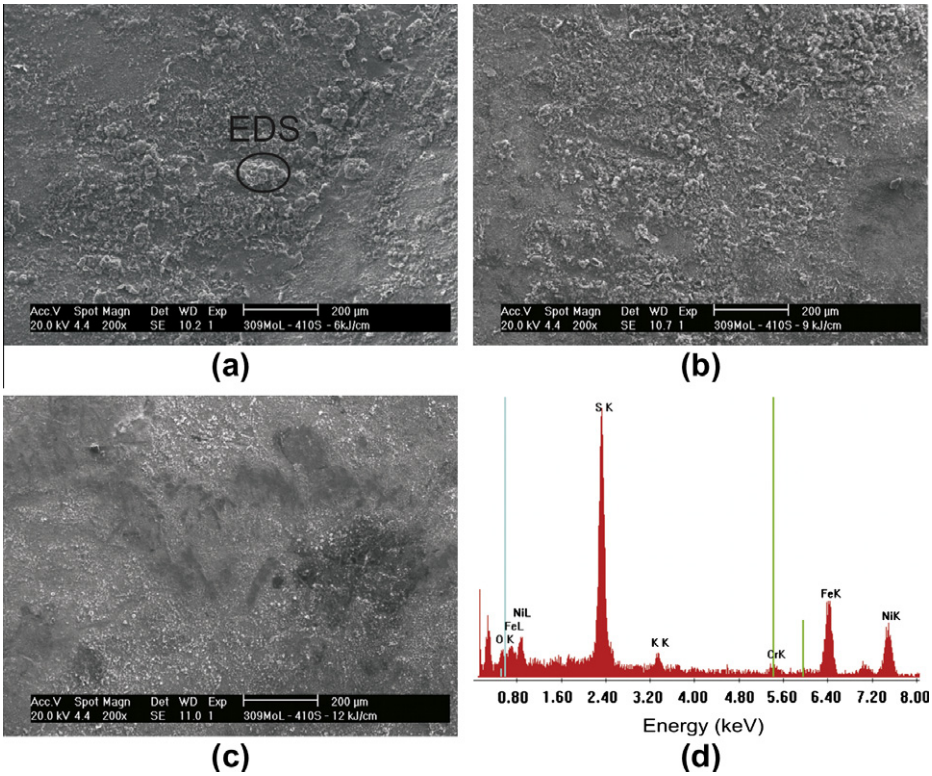

Fig. 7. Superficial characterization by SEM of the weld metal treated at 300 °C. (a) 6 kJ/cm. (b) 9 kJ/cm. (c) 12 kJ/cm. (d) EDS analysis of the iron sulfide layer indicated in a.

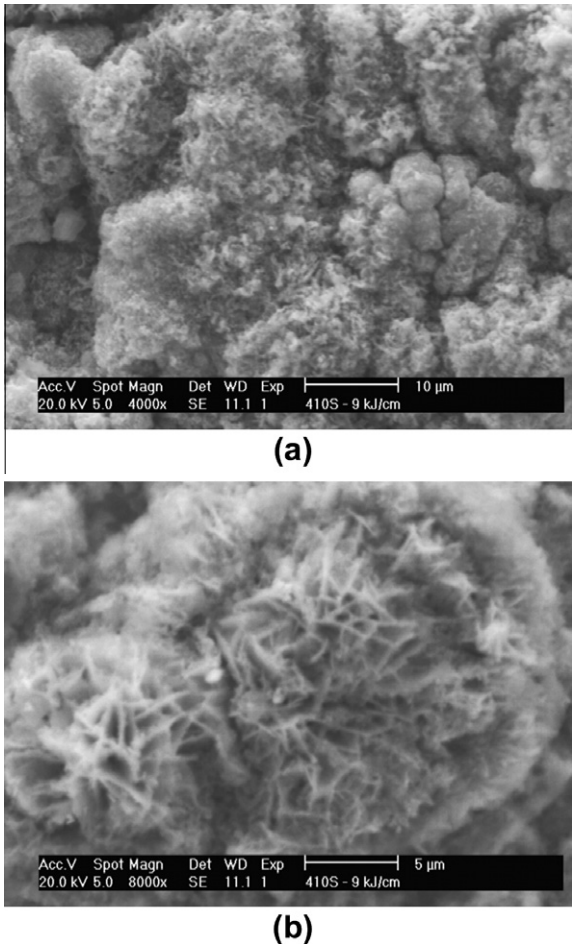

Fig. 8. Sample welded at 9 kJ/cm heat input energy. (a) Corrosion product layer. (b) Morphology detail of the corrosion product.

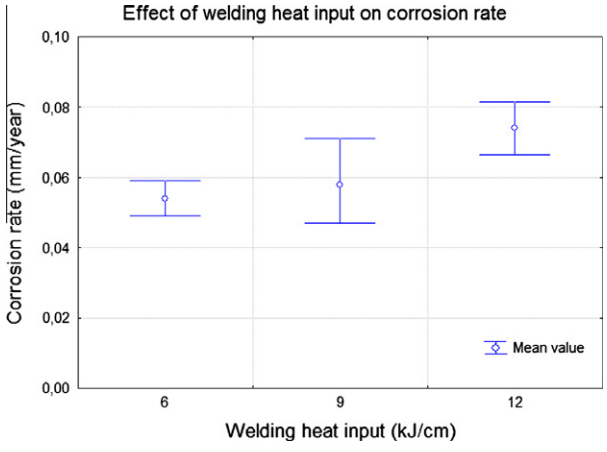

Fig. 9. Effect of welding heat input on weld metal corrosion rate.

(12.1 wt.%) to 8.54 wt.%, 8.04 wt.% and 7.39 wt.%, corresponding to a reduction of between 29.4% and 38.9% of the original level. The alterations in chemical composition do not significantly influence the corrosion resistance of the weld metal.

When the microstructure of the weld metal was diluted with AISI 410S stainless steel is evaluated, there is an increase in the levels of δ-ferrite with the increases in the welding heat input, therefore, the corrosion rates are apparently unaffected, as shown in Fig. 10. This behavior was quite different with that seen by Silva

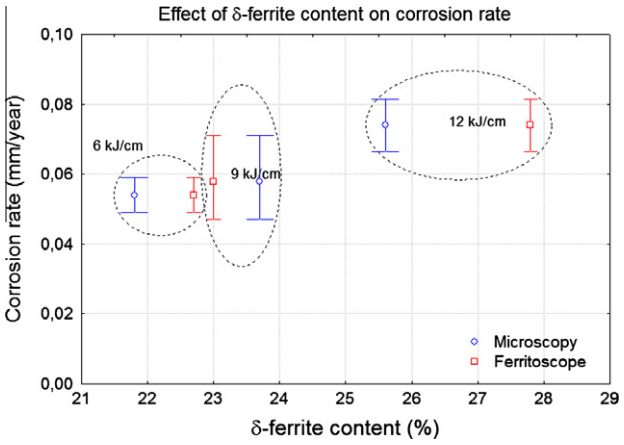

Fig. 10. Evaluation of corrosion resistance and microstructure relationship. Behavior of corrosion rate caused by the petroleum as a function of the δ-ferrite content in the weld metal.

et al. [3] in which the effect of δ-ferrite on corrosion resistance was attributed to the difference in the chemical composition between ferrite and austenite, due to segregation during solidification and partitioning due to phase transformation.

Regarding the resistance to corrosion, Delong [40] mentions that the presence of δ-ferrite in the weld metal has a neutral or modestly beneficial effect. Tuthill and Avery [41], studied the corrosion behavior of stainless steel and high alloys welded joints. They verified that the high δ-ferrite content was not related to the low corrosion resistance of the welded metal, which was attributed to the molybdenum and the chromium segregations. However, Manning et al. [42], studied localized corrosion in 304L stainless steels with a dual phase microstructure (δ-ferrite and austenite), which verified that pits occurred in the δ-ferrite/austenite interface; the explanation for this was the sulfur and phosphorous segregation in the interface.

It is well known that δ-ferrite is more rich in chromium content, this fact can explain its high resistance to corrosion when compared with austenite phase. Besides of that, the presence of two phases with different corrosion resistance can form an active–passive region, accelerating the attack on the austenite matrix. This characteristic was observed by Cui and Lundin [43] in the evaluation of pitting immersion performance of the AISI 316L stainless steel weld metal and shown that the preferential corrosion attack occurred in the austenite phase instead of ferrite phase. However, analysis performed by EDS indicated no significant change in chemical composition between ferrite and austenite in the weld metal.

4. Conclusions

Based on the experimental results obtained in the welding conditions and in the corrosion tests of petroleum at high temperature for austenitic–ferritic stainless steel dissimilar weld metal used in this study, it was possible to conclude that the AWS E309MoL stainless steel weld metal diluted with the AISI 410S stainless steel, has a typical δ-ferrite acicular morphology, which occurs in welds that solidify in primary ferrite mode (F). The level of δ-ferrite altered with the increases of the welding heat input, was due to the variations in the composition of the weld metal, caused by dilution. The material surface was corroded by acid present in the petroleum. The corrosion product formed in corroded surfaces, was only iron sulfide. In general, the corrosion rate in the weld metals evaluated was considered satisfactory with little variation between the welding heat inputs applied.

Acknowledgments

Authors are thankful to the following laboratories: Welding Engineering Laboratory (ENGESOLDA-UFC), Materials Characterization Laboratory (LACAM-UFC) and the Oils and Fuel Laboratory (LCL-UFC); also to the ACESITA S/A and CENPES/PETROBRAS for their collaboration, as well as for the financial support given by the Research and Projects Financing (FINEP), National Council for Research and Development (CNPq) and Coordination for the Improvement of People with Higher Education (CAPES).

References

[1] Silva CC, SanÍAna HB, Farias JP. Resistance evaluation of distillation tower welded metal plate linings to corrosion caused by heavy crude oil. Bol Tec Petrobras 2008;51:9–35 [in Portuguese].
[2] Sathiya P, Aravindan S, Noorul Haq A. Int J Adv Manuf Technol 2007;31:1076–82.
[3] Silva CC, de Miranda HC, de Sant'Ana HB, Farias JP. Microstructure, hardness and petroleum corrosion evaluation of 316L/AWS E309MoL-16 weld metal. Mater Charact 2009;60:346–52.
[4] Silva CC, de Sant'Ana HB, Farias JP. Evaluation of AISI 316L stainless steel welded plates in heavy petroleum environment. Mater Des 2009;30:1581–7.
[5] Machado JPSE, Silva CC, Sobral-Santiago AVC, de Sant'Ana HB, Farias JP. Effect of temperature on the level of corrosion caused by heavy petroleum on AISI 304 and AISI 444 stainless steel. Mater Res 2006;9:137–42.
[6] Folkhard E. Welding metallurgy of stainless steels. New York: Spring-Verlag Wien; 1988.
[7] Kou S. Welding metallurgy. New York: John Wiley & Sons; 1987.
[8] Liao J. Nitride precipitation in the weld HAZ of a duplex stainless steel. ISIJ Int 2001;41:460–7.
[9] Van Zwieten ACTM, Bulloch JH. Some considerations on the toughness properties of ferritic stainless steel – a brief review. Int J Press Vess Pipi 1993;56:1–31.
[10] Silva CC, Almeida Neto JC, Sant'Ana HB, Farias JP. Alterações Microestruturais na ZAC do Aço Inoxidável AISI 410S: Efeitos Sobre a Resistência à Corrosão. Sold Insp 2006;11:188–99 [in Portuguese].
[11] Silva CC, Guimarães RF, Menezes JWA, Miranda HC, Sant'Ana HB, Farias JP. Microstructural characterization of the HAZ in AISI 444 ferritic stainless steel welds. Mater Charact 2008;59:528–33.
[12] Shanmugam K, Lakshminarayanan AK, Balasubramania V. Tensile and impact properties of shielded metal arc welded AISI 409M ferritic stainless steel joints. J Mater Sci Technol 2009;25:181–6.
[13] Sathiya P, Aravindan S, Noorul Haq A. Effect of friction welding parameters on mechanical and metallurgical properties of ferritic stainless steel. Int J Adv Manuf Technol 2007;31:1076–82.
[14] Lakshminarayanan AK, Shanmugam K, Balasubramanian V. Effect of welding processes on tensile and impact properties, hardness and microstructure of AISI 409M ferritic stainless joints fabricated by duplex stainless steel filler metal. J Iron Steel Res Int 2009;16:66–72.
[15] Kotecki DJ. Stainless Q&A. Weld J 2005;84:14–6.
[16] Lakshminarayanan AK, Shanmugam K, Balasubramanian V. Fatigue crack growth behavior of gas metal arc welded AISI 409 grade ferritic stainless steel joints. J Mater Eng Perform 2009;18:917–24.
[17] Bala Srinivasan P, Satish Kumar MP. Characterisation of thin section dissimilar weld joint comprising austenitic and ferritic stainless steels. Mater Sci Technol 2008;24:392–8.
[18] Lakshminarayanan AK, Shanmugam K, Balasubramanian V. Effect of welding processes on fatigue crack growth behaviour of AISI 409M ferritic stainless steel joints fabricated using duplex stainless steel fillers. Fatigue Fract Eng Mater Struct 2009;32:656–64.
[19] Lakshminarayanan AK, Shanmugam K, Balasubramanian V. Effect of welding processes on tensile, impact, hardness and microstructure of joints made of AISI 409M FSS base metal and AISI 308L ASS filler metals. Ironmaking Steelmaking 2009;36:75–80.
[20] Silva CC, Machado JPSE, Farias JP, Sobral AVC, Sant'Ana HB, Rodrigues CEAL. Evaluation of AWS E309MoL-16 stainless steel weld metal corrosion in petroleum environment. Technol Metal Mater 2008;2:37–42.
[21] Bilmes P, González A, Liorente C, Solari M. Influencia de la Morfología de Solidificación de la Ferrita δ del Metal de Soldadura de Aceros Inoxidables Austeníticos Sobre las Propiedades de la Unión. Weld Res Abroad 1997;43:18–29.
[22] Elmer JW, Allen SM, Eagar TW. Microstructural development during solidification in stainless steel alloys. Metall Trans A 1989;20A:1989–2117.
[23] Silva CC, Machado JPSE, Sobral-Santiago AV, Sant'Ana HB, Farias JP. High-temperature hydrogen sulfide corrosion on the heat-affected zone of the AISI 444 stainless steel caused by venezuelan heavy petroleum. J Pet Sci Eng 2007;59:219–25.
[24] Albuquerque VHC, Silva CC, Menezes TIS, Farias JP, Tavares JMRS. Automatic evaluation of nickel alloy secondary phases from SEM images. Micros Res Technol 2011;74:36–46.
[25] Kotecki DJ, Siewert TA. WRC-1992 constitution diagram for stainless steel weld metals: a modification of the WRC-1988 diagram. Weld J 1992;71:171–8.
[26] Kotecki DJ. A martensite boundary on the WRC-1992 diagram. Weld J 1999;78:180–92.
[27] Rodrigues CEAL, de Azevedo AGL, Silva CC, Farias JP. Evaluation of the mechanical and metallurgical characteristics of weld metals deposited by class ANSI/AWS class A5.4-06 E309 covered electrodes. Weld Int 2009;23:237–50.
[28] Ogawa T, Koseki T. Effect of composition profiles on metallurgy and corrosion behavior of duplex stainless steel weld metals. Weld J 1989;68:181–91.
[29] David SA. Ferrite morphology and variations in ferrite content in austenitic stainless steel welds. Weld J 1981;60:63–71.
[30] Suutala N, Takalo T, Moisio T. Ferritic–austenitic solidification mode in austenitic stainless steel welds. Metall Trans A: Phys Metall Mater Sci 1980;11A:717–25.
[31] Lippold JC, Savage WF. Solidification of austenitic stainless steel weldments: Part 2 – The effect of alloy composition on ferrite morphology. Weld J 1980;59:48–58.
[32] Medvedeva ML. Specifics of high-temperature corrosion processes during oil recovery. Chem Pet Eng 2000;36:749–54.
[33] Craig H. Naphthenic acid corrosion in the refinery. In: Proc. conf. corrosion 95. Orlando (FL, USA): NACE; March 1995 [paper no. 333].
[34] Craig H. Temperature and velocity effects in naphthenic acid corrosion. In: Proc. conf. corrosion 96. Denver (CO, USA): NACE; March 1996 [paper no. 603].
[35] Babaian-Kibala E, Nugent MJ. Naphthenic acid corrosion literature survey. In: Proceedings of corrosion 99. NACE International; 1999 [paper no. 378].
[36] Tebbal S. Critical review of naphthenic acid corrosion. In: Proceedings of corrosion 99. NACE International; 1999 [paper no. 380].
[37] Slavcheva E, Shone B, Tumbull A. Review of naphthenic corrosion. Brit Corros J 1999;34:125–31.
[38] Piehl R. Naphthenic acid corrosion in crude distillation units. In: Proc. conf. corrosion 87. San Francisco (CA, USA): NACE; March 1987 [paper no. 196].
[39] Piehl R. Naphthenic acid corrosion in crude distillation units. Mater Perform 1988;44:37.
[40] Delong WT. Ferrite in austenitic stainless steel weld metal. Weld J 1974;53:273–86.
[41] Tuthill AH, Avery RE. Corrosion behavior of stainless steel and high alloy weldments in aggressive oxidizing environments. Weld J 1993;72:41–9.
[42] Manning PE, Duquette DJ, Savage WF. Technical note: the effect of retained ferrite on localized corrosion in duplex 304L stainless steel. Weld J 1980;59:260–2.
[43] Cui Y, Lundin CD. Austenite-preferential corrosion attack in 316 austenitic stainless steel weld metals. Mater Des 2007;28:324–8.